Vortices in Bose-Einstein Condensates: Theory

N. G. Parker[1], B. Jackson[2], A. M. Martin[1], and C. S. Adams[3]

[1] School of Physics, University of Melbourne, Parkville, Victoria 3010, Australia. `ngparker@ph.unimelb.edu.au,amm@ph.unimelb.edu.au`
[2] School of Mathematics and Statistics, Newcastle University, Newcastle upon Tyne, NE1 7RU, United Kingdom. `brian.jackson@newcastle.ac.uk`
[3] Department of Physics, Durham University, South Road, Durham, DH1 3LE, United Kingdom. `c.s.adams@durham.ac.uk`

1 Quantized vortices

Vortices are pervasive in nature, representing the breakdown of laminar fluid flow and hence playing a key role in turbulence. The fluid rotation associated with a vortex can be parameterized by the circulation $\Gamma = \oint d\mathbf{r} \cdot \mathbf{v}(\mathbf{r})$ about the vortex, where $\mathbf{v}(\mathbf{r})$ is the fluid velocity field. While classical vortices can take any value of circulation, superfluids are irrotational, and any rotation or angular momentum is constrained to occur through vortices with quantized circulation. Quantized vortices also play a key role in the dissipation of transport in superfluids. In BECs quantized vortices have been observed in several forms, including single vortices [1, 2], vortex lattices [3, 4, 5, 6] (see also Chap. VII), and vortex pairs and rings [7, 8, 9]. The recent observation of quantized vortices in a fermionic gas was taken as a clear signature of the underlying condensation and superfluidity of fermion pairs [10]. In addition to BECs, quantized vortices also occur in superfluid Helium [11, 12], nonlinear optics, and type-II superconductors [13].

1.1 Theoretical Framework

Quantization of circulation

Quantized vortices represent phase defects in the superfluid topology of the system. Under the Madelung transformation, the macroscopic condensate 'wavefunction' $\psi(\mathbf{r}, t)$ can be expressed in terms of a fluid density $n(\mathbf{r}, t)$ and a macroscopic phase $S(\mathbf{r}, t)$ via $\psi(\mathbf{r}) = \sqrt{n(\mathbf{r}, t)} \exp[iS(\mathbf{r}, t)]$. In order that the wavefunction remains single-valued, the change in phase around any closed contour C must be an integer multiple of 2π,

$$\int_C \nabla S \cdot d\mathbf{l} = 2\pi q, \tag{1}$$

where q is an integer. The gradient of the phase S defines the superfluid velocity via $\mathbf{v}(\mathbf{r}, t) = (\hbar/m)\nabla S(\mathbf{r}, t)$. This implies that the circulation about the contour C is given by,

$$\Gamma = \int_C \mathbf{v} \cdot d\mathbf{l} = q\left(\frac{h}{m}\right). \tag{2}$$

In other words, the circulation of fluid is quantized in units of (h/m). The circulating fluid velocity about a vortex is given by $\mathbf{v}(r, \theta) = q\hbar/(mr)\hat{\boldsymbol{\theta}}$, where r is the radius from the core and $\hat{\boldsymbol{\theta}}$ is the azimuthal unit vector.

Theoretical model

The Gross-Pitaevskii equation (GPE) provides an excellent description of BECs at the mean-field level in the limit of ultra-cold temperature [14]. It supports quantized vortices, and has been shown to give a good description of the static properties and dynamics of vortices [14, 15]. Dilute BECs require a confining potential, formed by magnetic or optical fields, which typically varies quadratically with position. We will assume an axially-symmetric harmonic trap of the form $V = \frac{1}{2}m(\omega_r^2 r^2 + \omega_z^2 z^2)$, where ω_r and ω_z are the radial and axial trap frequencies respectively. Excitation spectra of BEC states can be obtained using the Bogoliubov equations, and specify the stability of stationary solutions of the GPE. For example, the presence of the so-called anomalous modes of a vortex in a trapped BEC are indicative of their thermodynamic instability. The GPE can also give a qualitative, and sometimes quantitative, understanding of vortices in superfluid Helium [11, 12].

Although this Chapter deals primarily with vortices in repulsively-interacting BECs, vortices in attractively-interacting BECs have also received theoretical interest. The presence of a vortex in a trapped BEC with attractive interactions is less energetically favorable than for repulsive interactions [16]. Indeed, a harmonically-confined attractive BEC with angular momentum is expected to exhibit a center-of-mass motion rather than a vortex [17]. The use of anharmonic confinement can however support metastable vortices, as well as regimes of center-of-mass motion and instability [18, 19, 20].

Various approximations have been made to incorporate thermal effects into the GPE to describe vortices at finite temperature (see also Chap. XI). The Popov approximation self-consistently couples the condensate to a normal gas component using the Bogoliubov-de-Gennes formalism [21] (cf. Chap. I Sec. 5.2). Other approaches involve the addition of thermal/quantum noise to the system, such as the stochastic GPE method [22, 23, 24] and the classical field/truncated Wigner methods [25, 26, 27, 28]. Thermal effects can also be simulated by adding a phenomenological dissipation term to the GPE [29].

Basic properties of vortices

In a homogeneous system, a quantized vortex has the 2D form,

$$\psi(r,\theta) = \sqrt{n_{\mathrm{v}}(r)} \exp(iq\theta). \tag{3}$$

The vortex density profile $n_{\mathrm{v}}(r)$ has no analytic solution, although approximate solutions exist [30]. Vortex solutions can be obtained numerically by propagating the GPE in imaginary time $(t \to -it)$ [31], whereby the GPE converges to the lowest energy state of the system (providing it is stable). By enforcing the phase distribution of Eq. (3), a vortex solution is generated. Figure 1 shows the solution for a $q = 1$ vortex at the center of a harmonically-confined BEC. The vortex consists of a node of zero density with a width characterized by the condensate healing length $\xi = \hbar/\sqrt{mn_0 g}$, where $g = 4\pi\hbar^2 a/m$ (with a the s-wave scattering length) and n_0 is the peak density in the absence of the vortex. For typical BEC parameters [3], $\xi \sim 0.2~\mu m$. For a $q = 1$ vortex at the center of an axially-symmetric potential, each particle carries $\hbar$ of angular momentum. However, if the vortex is off-center, the angular momentum per particle becomes a function of position [15].

1.2 Vortex structures

Increasing the vortex charge widens the core due to centrifugal effects. In harmonically-confined condensates a multiply-quantized vortex with $q > 1$ is energetically unfavorable compared to a configuration of singly-charged vortices [32, 33]. Hence, a rotating BEC generally contains an array of singly-charged vortices in the form of a triangular Abrikosov lattice [3, 4, 5, 6, 34] (see also Chap. VII), similar to those found in rotating superfluid helium [11]. A $q > 1$ vortex can decay by splitting into singly-quantized vortices via a dynamical instability [35, 36], but is stable for some interaction strengths [37]. Multiply-charged vortices are also predicted to be stabilized by a suitable localized pinning potential [38] or the addition of quartic confinement [33].

Two-dimensional vortex-antivortex pairs (i.e. two vortices with equal but opposite circulation) and 3D vortex rings arise in the dissipation of superflow, and represent solutions to the homogeneous GPE in the moving frame [39, 40], with their motion being self-induced by the velocity field of the vortex lines. When the vortex lines are so close that they begin to overlap, these states are no longer stable and evolves into a rarefaction pulse [39].

Having more than one spin component in the BECs (cf. Chap. IX) provides an additional topology to vortex structures. Coreless vortices and vortex 'molecules' in coupled two-component BECs have been probed experimentally [41] and theoretically [42]. More exotic vortex structures such as skyrmion excitations [43] and half-quantum vortex rings [44] have also been proposed.

2 Nucleation of vortices

Vortices can be generated by rotation, a moving obstacle, or phase imprinting methods. Below we discuss each method in turn.

2.1 Rotation

As discussed in the previous section, a BEC can only rotate through the existence of quantized vortex lines. Vortex nucleation occurs only when the rotation frequency Ω of the container exceeds a critical value Ω_c [15, 32, 46]. Consider a condensate in an axially-symmetric trap which is rotating about the z-axis at frequency Ω. In the Thomas-Fermi limit, the presence of a vortex becomes energetically favorable when Ω exceeds a critical value given by [47],

$$\Omega_c = \frac{5}{2}\frac{\hbar}{mR^2}\ln\frac{0.67R}{\xi}.$$ (4)

This is derived by integrating the kinetic energy density $mn(r)v(r)^2/2$ of the vortex velocity field in the radial plane. The lower and upper limits of the integration are set by the healing length ξ and the BEC Thomas-Fermi radius R, respectively. Note that $\Omega_c < \omega_r$ for repulsive interactions, while $\Omega_c > \omega_r$ for attractive interactions [16]. In a non-rotating BEC the presence of a vortex raises the energy of the system, indicating thermodynamic instability [48].

In experiments, vortices are formed only when the trap is rotated at a much higher frequency than Ω_c [3, 4, 5], demonstrating that the energetic criterion is a necessary, but not sufficient, condition for vortex nucleation. There must also be a dynamic route for vorticity to be introduced into the condensate, and hence Eq. (4) provides only a lower bound for the critical frequency.

The nucleation of vortices in rotating trapped BECs appears to be linked to instabilities of collective excitations. Numerical simulations based on the GPE have shown that once the amplitude of these excitations become sufficiently large, vortices are nucleated that subsequently penetrate the high-density bulk of the condensate [23, 27, 29, 49, 50].

One way to induce instability is to resonantly excite a surface mode by adding a rotating deformation to the trap potential. In the limit of small perturbations, this resonance occurs close to a rotation frequency $\Omega_r = \omega_\ell/\ell$, where ω_ℓ is the frequency of a surface mode with multipolarity ℓ. In the Thomas-Fermi limit, the surface modes satisfy $\omega_\ell = \sqrt{\ell}\omega_r$ [51], so $\Omega_r = \omega_r/\sqrt{\ell}$. For example, an elliptically-deformed trap, which excites the $\ell = 2$ quadrupole mode, would nucleate vortices when rotated at $\Omega_r \approx \omega_r/\sqrt{2}$. This value has been confirmed in both experiments [3, 4, 5] and numerical simulations [23, 27, 29, 49, 50]. Higher multipolarities were resonantly excited in the experiment of Ref. [6], finding vortex formation at frequencies close to the expected values, $\Omega = \omega_r/\sqrt{\ell}$, and lending further support to this picture.

A similar route to vortex nucleation is revealed by considering stationary states of the BEC in a rotating elliptical trap, which can be obtained in the Thomas-Fermi limit by solving hydrodynamic equations [52]. At low rotation rates only one solution is found; however at higher rotations ($\Omega > \omega_r/\sqrt{2}$) a bifurcation occurs and up to three solutions are present. Above the bifurcation point one or more of the solutions become dynamically unstable [53], leading

to vortex formation [54]. Madison *et al.* [55] followed these stationary states experimentally by adiabatically introducing trap ellipticity and rotation, and observed vortex nucleation in the expected region.

Surface mode instabilities can also be induced at finite temperature by the presence of a rotating noncondensed "thermal" cloud. Such instabilities occur when the thermal cloud rotation rate satisfies $\Omega > \omega_\ell/\ell$ [56]. Since all modes can potentially be excited in this way, the criterion for instability and hence vortex nucleation becomes $\Omega_c > \min(\omega_\ell/\ell)$, analogous to the Landau criterion. Note that such a minimum exists at $\Omega_c > 0$ since the Thomas-Fermi result $\omega_\ell = \sqrt{\ell}\omega_r$ becomes less accurate for high ℓ [57]. This mechanism may have been important in the experiment of Haljan *et al.* [34], where a vortex lattice was formed by cooling a rotating thermal cloud to below T_c.

2.2 Nucleation by a moving object

Vortices can also be nucleated in BECs by a moving localized potential. This problem was originally studied using the GPE for 2D uniform condensate flow around a circular hard-walled potential [58, 59], with vortex-antivortex pairs being nucleated when the flow velocity exceeded a critical value.

In trapped BECs a similar situation can be realized using the optical dipole force from a laser, giving rise to a localized repulsive Gaussian potential. Under linear motion of such a potential, numerical simulations revealed vortex pair formation when the potential is moved at a velocity above a critical value [60]. The experiments of [61, 62] oscillated a repulsive laser beam in an elongated condensate. Although vortices were not observed directly, the measurement of condensate heating and drag above a critical velocity was consistent with the nucleation of vortices [63].

An alternative approach is to move the laser beam potential in a circular path around the trap center [64]. By "stirring" the condensate in this way one or more vortices can be created. This technique was used in the experiment of Ref. [6], where vortices were generated even at low stirring frequencies.

2.3 Other mechanisms and structures

A variety of other schemes for vortex creation have been suggested. One of the most important is that by Williams and Holland [65], who proposed a combination of rotation and coupling between two hyperfine levels to create a two-component condensate, one of which is in a vortex state. The non-vortex component can then either be retained or removed with a resonant laser pulse. This scheme was used by the first experiment to obtain vortices in BEC [1]. A related method, using topological phase imprinting, has been used to experimentally generate multiply-quantized vortices [66].

Apart from the vortex lines considered so far, vortex rings have also been the subject of interest. Rings are the decay product of dynamically unstable dark solitary waves in 3D geometries [7, 8, 67, 68]. Vortex rings also form

in the quantum reflection of BECs from surface potentials [69], the unstable motion of BECs through an optical lattice [70], the dragging of a 3D object through a BEC [71], and the collapse of ultrasound bubbles in BECs [72]. The controlled generation of vortex rings [73] and multiple/bound vortex ring structures [74] have been analyzed theoretically.

A finite temperature state of a quasi-2D BEC, characterized by the thermal activation of vortex-antivortex pairs, has been simulated using classical field simulations [75]. This effect is thought to be linked to the Berezinskii-Kosterlitz-Thouless phase transition of 2D superfluids, recently observed experimentally in ultracold gases [76]. Similar simulations in a 3D system have also demonstrated the thermal creation of vortices [77, 78].

3 Dynamics of vortices

The study of vortex dynamics has long been an important topic in both classical [79] and quantum [12] hydrodynamics. Helmholtz's theorem for uniform, inviscid fluids, which is also applicable to quantized vortices in superfluids near zero temperature, states that the vortex will follow the motion of the background fluid. So, for example, in a superfluid with uniform flow velocity $\mathbf{v}_s$, a single straight vortex line will move with velocity $\mathbf{v}_L$, such that it is stationary in the frame of the superfluid.

Vortices similarly follow the "background flow" originating from circulating fluid around a vortex core. Hence vortex motion can be induced by the presence of other vortices, or by other parts of the same vortex line when it is curved. Most generally, the superfluid velocity $\mathbf{v}_i$ due to vortices at a particular point $\mathbf{r}$ is given by the *Biot-Savart* law [12], in analogy with the similar equation in electromagnetism,

$$\mathbf{v}_i = \frac{\Gamma}{4\pi} \int \frac{(\mathbf{s} - \mathbf{r}) \times d\mathbf{s}}{|\mathbf{s} - \mathbf{r}|^3};$$
(5)

where $\mathbf{s}(\zeta, t)$ is a curve representing the vortex line with ζ the arc length. Equation (5) suffers from a divergence at $\mathbf{r} = \mathbf{s}$, so in calculations of vortex dynamics this must be treated carefully [80]. Equation (5) also assumes that the vortex core size is small compared to the distance between vortices. In particular, it breaks down when vortices cross during collisions, where reconnection events can occur. These reconnections can either be included manually [81], or by solving the full GPE [82]. The latter method also has the advantage of including sound emission due to vortex motion or reconnections [83, 84].

In a system with multiple vortices, motion of one vortex is induced by the circulating fluid flow around other vortices, and vice-versa [11]. This means that, for example, a pair of vortices of equal but opposite charge will move linearly and parallel to each other with a velocity inversely proportional to the distance between them. Two or more vortices of equal charge, meanwhile,

will rotate around each other, giving rise to a rotating vortex lattice as will be discussed in Chap. VII. When a vortex line is curved, circulating fluid from one part of the line can induce motion in another. This effect can give rise to helical waves on the vortex, known as Kelvin modes [85]. It also has interesting consequences for a vortex ring, which will travel in a direction perpendicular to the plane of the ring, with a self-induced velocity that decreases with increasing radius. Classically, this is most familiar in the motion of smoke rings, though similar behavior has also been observed in superfluid helium [86].

This simple picture is complicated in the presence of density inhomogeneities or confining walls. In a harmonically-trapped BEC the density is a function of position, and therefore the energy, E, of a vortex will also depend on its position within the condensate. To simplify matters, let us consider a quasi-2D situation, where the condensate is pancake-shaped and the vortex line is straight. In this case, the energy of the vortex depends on its displacement $\mathbf{r}$ from the condensate center [87], and a displaced vortex feels a force proportional to ∇E. This is equivalent to a Magnus force on the vortex [88, 89, 90] and to compensate the vortex moves in a direction perpendicular to the force, leading it to precess around the center of the condensate along a line of constant energy. This precession of a single vortex has been observed experimentally [2], with a frequency in agreement with theoretical predictions. In more 3D situations, such as spherical or cigar-shaped condensates, the vortex can bend [91, 92, 93, 94] leading to more complicated motion [15]. Kelvin modes [95, 96] and vortex ring dynamics [88] are also modified by the density inhomogeneity in the trap.

In the presence of a hard-wall potential, a new constraint is imposed such that the fluid velocity normal to the wall must be zero, $\mathbf{v}_s \cdot \hat{\mathbf{n}} = 0$. The resulting problem of vortex motion is usually solved mathematically [79] by invoking an "image vortex" on the other side of the wall (i.e. in the region where there is no fluid present), at a position such that its normal flow cancels that of the real vortex at the barrier. The motion of the real vortex is then simply equal to the induced velocity from the image vortex circulation.

4 Stability of vortices

4.1 Thermal instabilities

At finite temperatures the above discussion is modified by the thermal occupation of excited modes of the system, which gives rise to a noncondensed normal fluid in addition to the superfluid. A vortex core moving relative to the normal fluid scatters thermal excitations, and will therefore feel a frictional force leading to dissipation. This mutual friction force can be written as [11],

$$\mathbf{f}_D = -n_s \Gamma \{\alpha \mathbf{s}' \times [\,\mathbf{s}' \times (\mathbf{v}_n - \mathbf{v}_L)] + \alpha' \mathbf{s}' \times (\mathbf{v}_n - \mathbf{v}_L)\}, \qquad (6)$$

where n_s is the background superfluid density, $\mathbf{s}'$ is the derivative of $\mathbf{s}$ with respect to arc length ζ, α and α' are temperature dependent parameters,

while $\mathbf{v}_L$ and $\mathbf{v}_n$ are the velocities of the vortex line and normal fluid respectively. The mutual friction therefore has two components perpendicular to the relative velocity $\mathbf{v}_n - \mathbf{v}_L$.

To consider an example discussed in the last section, an off-center vortex in a trapped BEC at zero temperature will precess such that its energy remains constant. In the presence of a non-condensed component, however, dissipation will lead to a loss of energy. Since the vortex is topological it cannot simply vanish, so this lost energy is manifested as a radial drift of the vortex towards lower densities. In Eq. (6) the α term is responsible for this radial motion, while α' changes the precession frequency. The vortex disappears at the edge of the condensate, where it is thought to decay into elementary excitations [97]. Calculations based upon the stochastic GPE have shown that thermal fluctuations lead to an uncertainty in the position of the vortex, such that even a central vortex will experience thermal dissipation and have a finite lifetime [24]. This thermodynamic lifetime is predicted to be of the order of seconds [97], which is consistent with experiments [1, 3, 94].

4.2 Hydrodynamic instabilities

Experiments indicate that the crystallization of vortex lattices is temperature-independent [5, 98]. Similarly, vortex tangles in turbulent states of superfluid Helium have been observed to decay at ultracold temperature, where thermal dissipation is virtually nonexistent [99]. These results highlight the occurrence of zero temperature dissipation mechanisms, as listed below.

Instability to acceleration

The topology of a 2D homogeneous superfluid can be mapped on to a (2+1)D electrodynamic system, with vortices and phonons playing the role of charges and photons respectively [100]. Just as an accelerating electron radiates according to the Larmor acceleration squared law, a superfluid vortex is inherently unstable to acceleration and radiates sound waves.

Vortex acceleration can be induced by the presence of an inhomogeneous background density, such as in a trapped BEC. Sound emission from a vortex in a BEC can be probed by considering a trap of the form [45],

$$V_{\text{ext}} = V_0 \left[1 - \exp\left(-\frac{m\omega_{\text{d}}^2 r^2}{2V_0} \right) \right] + \frac{1}{2}m\omega_r^2 r^2. \qquad (7)$$

This consists of a gaussian dimple trap with depth V_0 and harmonic frequency component ω_{d}, embedded in an ambient harmonic trap of frequency ω_r. A 2D description is sufficient to describe this effect. This set-up can be realized with a quasi-2D BEC by focussing a far-off-resonant red-detuned laser beam in the center of a magnetic trap. The vortex is initially confined in the inner region, where it precesses due to the inhomogeneous density. Since sound excitations
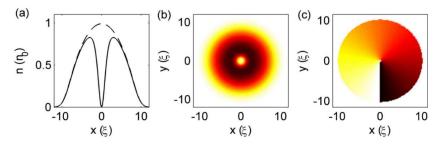
Fig. 1. Profile of a singly-quantized ($q = 1$) vortex at the center of a harmonically-confined BEC: (a) condensate density along the $y = 0$ axis (solid line) and the corresponding density profile in the absence of the vortex (dashed line). (b) 2D density and (c) phase profile of the vortex state. These profiles are calculated numerically by propagating the 2D GPE in imaginary time subject to an azimuthal 2π phase variation around the trap center.
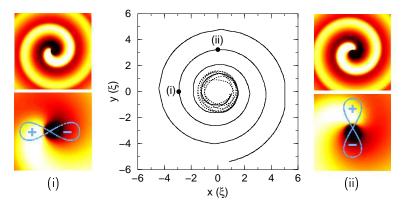

Fig. 2. Vortex path in the dimple trap geometry of Eq. (7) with $\omega_d = 0.28(c/\xi)$. Deep $V_0 = 10\mu$ dimple (dotted line): mean radius is constant, but modulated by the sound field. Shallow $V_0 = 0.6\mu$ dimple and homogeneous outer region $\omega_r = 0$ (dotted line): vortex spirals outwards. Outer plots: Sound excitations (with amplitude $\sim 0.01n_0$) radiated in the $V_0 = 0.6\mu$ system at times indicated. Top: Far-field distribution $[-90, 90]\xi \times [-90, 90]\xi$. Bottom: Near-field distribution $[-25, 25]\xi \times [-25, 25]\xi$, with an illustration of the dipolar radiation pattern. Copyright (2004) by the American Physical Society [45].

have an energy of the order of the chemical potential μ, the depth of the dimple relative to μ leads to two distinct regimes of vortex-sound interactions.

$V_0 \gg \mu$: The vortex effectively sees an infinite harmonic trap - it precesses and radiates sound but there is no net decay due to complete sound reabsorption. However, a collective mode of the background fluid is excited, inducing slight modulations in the vortex path (dotted line in Fig 2).

$V_0 < \mu$: Sound waves are radiated by the precessing vortex. Assuming $\omega_r = 0$, the sound waves propagate to infinity without reinteracting with the vortex.

The ensuing decay causes the vortex to drift to lower densities, resulting in a spiral motion (solid line in Fig. 2), similar to the effect of thermal dissipation. The sound waves are emitted in a dipolar radiation pattern, perpendicularly to the instantaneous direction of motion (subplots in Fig. 2), with a typical amplitude of order $0.01n_0$ and wavelength $\lambda \sim 2\pi c/\omega_V$ [15], where c is the speed of sound and ω_V is the vortex precession frequency. The power radiated from a vortex can be expressed in the form [45, 101, 102],

$$P = \beta m N \left(\frac{a^2}{\omega_V} \right), \tag{8}$$

where a is the vortex acceleration, N is the total number of atoms, and β is a dimensionless coefficient. Using classical hydrodynamics [101] and by mapping the superfluid hydrodynamic equations onto Maxwell's electrodynamic equations [102], it has been predicted that $\beta = \pi^2/2$ under the assumptions of a homogeneous 2D fluid, a point vortex, and perfect circular motion. Full numerical simulations of the GPE based on a realistic experimental scenario have derived a coefficient of $\beta \sim 6.3 \pm 0.9$ (one standard deviation), with the variation due to a weak dependence on the geometry of the system [45].

When $\omega_r \neq 0$, the sound eventually reinteracts with the vortex, slowing but not preventing the vortex decay. By varying V_0 it is possible to control vortex decay, and in suitably engineered traps this decay mechanism is expected to dominate over thermal dissipation [45].

Vortex acceleration (and sound emission) can also be induced by the presence of other vortices. A co-rotating pair of two vortices of equal charge has been shown to decay continuously via quadrupolar sound emission, both analytically [103] and numerically [104]. Three-body vortex interactions in the form of a vortex-antivortex pair incident on a single vortex have also been simulated numerically, with the interaction inducing acceleration in the vortices with an associated emission of sound waves [104].

Simulations of vortex lattice formation in a rotating elliptical trap show that vortices are initially nucleated in a turbulent disordered state, before relaxing into an ordered lattice [50]. This relaxation process is associated with an exchange of energy from the sound field to the vortices due to these vortex-sound interactions. This agrees with the experimental observation that vortex lattice formation is insensitive to temperature [5, 98].

Kelvin wave radiation and vortex reconnections

In 3D a Kelvin wave excitation will induce acceleration in the elements of the vortex line, and therefore local sound emission. Indeed, simulations of the GPE in 3D have shown that Kelvin waves excitations on a vortex ring lead to a decrease in the ring size, indicating the underlying radiation process [84]. Kelvin wave excitations can be generated from a vortex line reconnection [83, 84] and the interaction of a vortex with a rarefaction pulse [105].

Vortex lines which cross each other can undergo dislocations and reconnections [106], which induce a considerable burst of sound emission [83]. Although they have yet to be probed experimentally in BECs, vortex reconnections are hence thought to play a key role in the dissipation of vortex tangles in Helium II at ultra-low temperatures [11].

5 Dipolar BECs

A BEC has recently been formed of chromium atoms [107], which feature a large dipole moment. This opens the door to studying of the effect of long-range dipolar interactions in BECs.

5.1 The Modified Gross-Pitaevskii Equation

The interaction potential $U_{dd}(\mathbf{r})$ between two dipoles separated by $\mathbf{r}$, and aligned by an external field along the unit vector $\hat{\mathbf{e}}$ is given by,

$$U_{dd}(\mathbf{r}) = \frac{C_{dd}}{4\pi}\hat{e}_i\hat{e}_j\frac{(\delta_{ij} - 3\hat{r}_i\hat{r}_j)}{r^3}. \tag{9}$$

For low energy scattering of two atoms with dipoles induced by a static electric field $\mathbf{E} = E\hat{\mathbf{e}}$, the coupling constant $C_{dd} = E^2\alpha^2/\epsilon_0$ [108, 109], where α is the static dipole polarizability of the atoms and ϵ_0 is the permittivity of free space. Alternatively, if the atoms have permanent magnetic dipoles, d_m, aligned in an external magnetic field $\mathbf{B} = B\hat{\mathbf{e}}$, one has $C_{dd} = \mu_0 d_m^2$ [110], where μ_0 is the permeability of free space. Such dipolar interactions give rise to a mean-field potential

$$\Phi_{dd}(\mathbf{r}) = \int d^3r U_{dd}\left(\mathbf{r} - \mathbf{r}'\right)|\psi\left(\mathbf{r}'\right)|^2, \tag{10}$$

which can be incorporated into the GPE to give,

$$i\hbar\psi_t = \left[-\frac{\hbar^2}{2m}\nabla^2 + g|\psi|^2 + \Phi_{dd} + V\right]\psi. \tag{11}$$

For an axially-symmetric quasi-2D geometry ($\omega_z \gg \omega_r$) rotating about the z-axis, the ground state wavefunction of a single vortex has been solved numerically [111]. Considering 10^5 chromium atoms and $\omega_r = 2\pi \times 100$Hz, several solutions were obtained depending on the strength of the s-wave interactions and the alignment of the dipoles relative to the trap.

For the case of axially-polarized dipoles the most striking results arise for attractive s-wave interactions $g < 0$. Here the BEC density is axially symmetric and oscillates in the vicinity of the vortex core. Similar density oscillations have been observed in numerical studies of other non-local interaction potentials, employed to investigate the interparticle interactions in ^{4}He

[112, 113, 114, 115], with an interpretation that relates to the roton structure in a superfluid [115]. For the case of transversely-polarized dipoles, where the polarizing field is co-rotating with the BEC, and repulsive s-wave interactions ($g > 0$), the BEC becomes elongated along the axis of polarization [116] and as a consequence the vortex core is anisotropic.

5.2 Vortex Energy

Assuming a dipolar BEC in the TF limit (cf. Sec. 5.1 in Chap. I), the energetic cost of a vortex, aligned along the axis of polarization (z-axis), has been derived using a variational ansatz for the vortex core [117], and thereby the critical rotation frequency Ω_c at which the presence of a vortex becomes energetically favorable has been calculated. For an oblate trap ($\omega_r < \omega_z$), dipolar interactions decrease Ω_c, while for prolate traps ($\omega_r > \omega_z$) the presence of dipolar interactions increases Ω_c. A formula resembling Eq. (4) for the critical frequency of a conventional BEC can be used to explain these results, with R being the modified TF radius of the dipolar BEC. Indeed, using the TF radius of a vortex-free dipolar BEC [118, 119] and the conventional s-wave healing length ξ, it was found that Eq. (4) closely matches the results from the energy cost calculation. Deviations become significant when the dipolar interactions dominate over s-wave interactions. In this regime the s-wave healing length ξ is no longer the relevant length scale of the system, and the equivalent dipolar length scale $\xi_d = C_{dd} m / (12 \pi \hbar^2)$ will characterize the vortex core size.

For $g > 0$ and in the absence of dipolar interactions, the rotation frequency at which the vortex-free BEC becomes dynamically unstable, Ω_{dyn}, is always greater than the critical frequency for vortex stabilization Ω_c. However in the presence of dipolar interactions, Ω_{dyn} can become less than Ω_c, leading to an intriguing regime in which the dipolar BEC is dynamically unstable but vortices will not enter [117, 120]. As with attractive condensates [17], the angular momentum may then be manifested as center of mass oscillations.

6 Analogs of Gravitational Physics in BECs

There is growing interest in pursuing analogs of gravitational physics in condensed matter systems [121], such as BECs. The rationale behind such models can be traced back to the work of Unruh [122, 123], who noted the analogy between sound propagation in an inhomogeneous background flow and field propagation in curved space-time. This link applies in the TF limit of BECs where the speed of sound is directly analogous to the speed of light in the corresponding gravitational system [124]. This has led to proposals for experiments to probe effects such as Hawking radiation [125, 126] and superradiance [127]. For Hawking radiation it is preferable to avoid the generation of vortices [121, 128], and as such will not be discussed here. However, the phenomena

of superradiance in BECs, which can be considered as stimulated Hawking radiation, relies on the presence of a vortex [129, 130, 131, 132], which is analogous to a rotating black hole.

Below we outline the derivation of how the propagation of sound in a BEC can be considered to be analogous to field propagation [121]. From the GPE it is possible to derive the continuity equation for an irrotational fluid flow with phase $S(\mathbf{r}, t)$ and density $n(\mathbf{r}, t)$, and a Hamilton-Jacobi equation whose gradient leads to the Euler equation. Linearizing these equations with respect to the background it is found that

$$\partial_t S' = -\frac{1}{m}\nabla S \cdot \nabla S' - gn' + \frac{\hbar^2}{4m\sqrt{n}}\left(\nabla^2\frac{n'}{\sqrt{n}} - \frac{n'}{n}\nabla^2\sqrt{n}\right), \qquad (12)$$

$$\partial_t n' = -\frac{1}{m}\nabla \cdot (n\nabla S') - \frac{1}{m}\nabla \cdot (n'\nabla S), \qquad (13)$$

where n' and S' are the perturbed values of the density n and phase S respectively. Neglecting the quantum pressure ∇^2-terms, the above equations can be rewritten as a covariant differential equation describing the propagation of phase oscillations in a BEC. This is directly analogous to the propagation of a minimally coupled massless scalar field in an effective Lorentzian geometry which is determined by the background velocity, density and speed of sound in the BEC. Hence, the propagation of sound in a BEC can be used as an analogy for the propagation of electromagnetic fields in the corresponding space-time. Of course one has to be aware that this direct analogy is only valid in the TF regime, which breaks down on scales of the order of a healing length, i.e. the theory is only valid on large length scales, as is general relativity.

6.1 Superradiance

Superradiance in BECs relies on sound waves incident on a vortex structure and is characterized by the reflected sound energy exceeding the incident energy. This has been studied using Eqs. (12) and (13) for monochromatic sound waves of frequency ω_s and angular wave number q_s incident upon a vortex [129] and a 'draining vortex" (a vortex with outcoupling at its center) [130, 131, 132].

For the vortex case, a vortex velocity field $\mathbf{v}(r, \theta) = (\beta/r)\hat{\boldsymbol{\theta}}$ and a density profile ansatz was assumed. Superradiance then occurs when $\beta q_s > A c_\infty$, where A is related to the vortex density ansatz and c_∞ is the speed of sound at infinity [129]. Interestingly, this condition is frequency independent.

For the case of a draining vortex, an event horizon occurs at a distance a from the vortex core, where the fluid circulates at frequency Ω. Assuming a homogeneous density n and a velocity profile $\mathbf{v}(r, \theta) = \left(-ca\hat{\mathbf{r}} + \Omega a^2\hat{\boldsymbol{\theta}}\right)/r$ where c is the homogeneous speed of sound, superradiance occurs when $0 < \omega_s < q_s\Omega$ [130, 131, 132].

The increase in energy of the outgoing sound is due to an extraction of energy from the vortex and as such it is expected to lead to slowing of the

vortex rotation. However, such models do not include quantized vortex angular momentum, and as such it is expected that superradiance will be suppressed [132]. This raises tantalizing questions, such as whether superradiance can occur if vorticity is quantized, if such effects can be modeled with the GPE, and whether the study of quantum effects in condensate superradiance will shed light on quantum effects in general relativity.

References

1. M. R. Matthews, B. P. Anderson, P. C. Haljan, D. S. Hall, C. E. Wieman, and E. A. Cornell, Phys. Rev. Lett. **83**, 2498 (1999).
2. B. P. Anderson, P. C. Haljan, C. E. Wieman, and E. A. Cornell, Phys. Rev. Lett. **85**, 2857 (2000).
3. K. W. Madison, F. Chevy, W. Wohlleben, and J. Dalibard, Phys. Rev. Lett. **84**, 806 (2000).
4. J. R. Abo-Shaeer, C. Raman, J. M. Vogels, and W. Ketterle, Science **292**, 476 (2001).
5. E. Hodby, C. Hechenblaikner, S. A. Hopkins, O. M. Maragò, and C. J. Foot, Phys. Rev. Lett. **88**, 010405 (2002).
6. C. Raman, J. R. Abo-Shaeer, J. M. Vogels, K. Xu, and W. Ketterle, Phys. Rev. Lett. **87**, 210402 (2001).
7. B. P. Anderson, P. C. Haljan, C. A. Regal, D. L. Feder, L. A. Collins, C. W. Clark, and E. A. Cornell, Phys. Rev. Lett. **86**, 2926 (2001).
8. Z. Dutton, M. Budde, C. Slowe, and L. V. Hau, Science **293**, 663 (2001).
9. S. Inouye, S. Gupta, T. Rosenband, A. P. Chikkatur, A. Görlitz, T. L. Gustavson, A. E. Leanhardt, D. E. Pritchard, and W. Ketterle, Phys. Rev. Lett. **87**, 080402 (2001).
10. M. W. Zwierlein, J. R. Abo-Shaeer, A. Schirotzek, C. H. Schunck, and W. Ketterle, Nature **435**, 1047 (2005).
11. R. J. Donnelly: *Quantized vortices in Helium II* (Cambridge University Press, Cambridge, 1991).
12. C. F. Barenghi, R. J. Donnelly, and W. F. Vinen (Eds.): *Quantized Vortex Dynamics and Superfluid Turbulence* (Springer Verlag, Berlin, 2001).
13. D. R. Tilley and J. Tilley: *Superfluidity and Superconductivity* (IOP, Bristol, 1990).
14. F. Dalfovo, S. Giorgini, L. P. Pitaevskii, and S. Stringari, Rev. Mod. Phys. **71**, 463 (1999).
15. A. L. Fetter and A. A. Svidzinsky, J. Phys.: Condens. Matter **13**, R135 (2001).
16. F. Dalfovo and S. Stringari, Phys. Rev. A **53**, 2477 (1996).
17. N. K. Wilkin, J. M. F. Gunn, and R. A. Smith, Phys. Rev. Lett. **80**, 2265 (1998).
18. H. Saito and M. Ueda, Phys. Rev. A **69**, 013604 (2004).
19. E. Lundh, A. Collin, and K-A. Suominen, Phys. Rev. Lett. **92**, 070401 (2004).
20. G. M. Kavoulakis, A. D. Jackson, and G. Baym, Phys. Rev. A **70**, 043603 (2004).
21. S. M. M. Virtanen, T. P. Simula, M. M. Salomaa, Phys. Rev. Lett. **86**, 2704 (2001).

22. C. W. Gardiner, J. R. Anglin, and T. I. A. Fudge, J. Phys. B **35**, 1555 (2002).
23. A. A. Penckwitt, R. J. Ballagh, and C. W. Gardiner, Phys. Rev. Lett. **89**, 260402 (2002).
24. R. A. Duine, B. W. A. Leurs, and H. T. C. Stoof, Phys. Rev. A **69**, 053623 (2004).
25. M. J. Steel, M. K. Olsen, L. I. Plimak, P. D. Drummond, S. M. Tan, M. J. Collett, D. F. Walls, and R. Graham, Phys. Rev. A **58**, 4824 (1998).
26. M. J. Davis, S. A. Morgan, and K. Burnett, Phys. Rev. A **66**, 053618 (2002).
27. C. Lobo, A. Sinatra, and Y. Castin, Phys. Rev. Lett. **92**, 020403 (2004).
28. T. P. Simula and P. B. Blakie, Phys. Rev. Lett. **96**, 020404 (2006).
29. M. Tsubota, K. Kasamatsu, and M. Ueda, Phys. Rev. A **65**, 023603 (2002).
30. C. J. Pethick and H. Smith: *Bose-Einstein Condensation in Dilute Gases* (Cambridge, 2002).
31. A. Minguzzi, S. Succi, F. Toschi, M. P. Tosi, and P. Vignolo, Phys. Rep. **395**, 223 (2004).
32. D. A. Butts and D. S. Rokshar, Nature **397**, 327 (1999).
33. E. Lundh, Phys. Rev. A **65**, 043604 (2002).
34. P. C. Haljan, I. Coddington, P. Engels, and E. A. Cornell, Phys. Rev. Lett. **87**, 210403 (2001).
35. M. Möttönen, T. Mizushima, T. Isoshima, M. M. Salomaa, and K. Machida, Phys. Rev. A **68**, 023611 (2003).
36. Y. Shin, M. Saba, A. Schirotzek, T. A. Pasquini, A. E. Leanhardt, D. E. Pritchard, and W. Ketterle, Phys. Rev. Lett. **93**, 160406 (2004).
37. H. Pu, C. K. Law, J. H. Eberly, and N. P. Bigelow, Phys. Rev. Lett. **59**, 1533 (1999).
38. T. P. Simula, S. M. M. Virtanen, and M. M. Salomaa, Phys. Rev. A **65**, 033614 (2002).
39. C. A. Jones and P. H. Roberts, J. Phys. A **15**, 2599 (1982).
40. C. A. Jones, S. J. Putterman, and P. H. Roberts, J. Phys. A **19**, 2991 (1986).
41. A. E. Leanhardt, Y. Shin, D. Kielpinski, D. E. Pritchard, and W. Ketterle, Phys. Rev. Lett. **90**, 140403 (2003).
42. K. Kasamatsu, M. Tsubota, and M. Ueda, Phys. Rev. Lett. **93**, 250406 (2004).
43. J. Ruostekoski and J. R. Anglin, Phys. Rev. Lett. **86**, 003934 (2001).
44. J. Ruostekoski and J. R. Anglin, Phys. Rev. Lett. **91**, 190402 (2003).
45. N. G. Parker, N. P. Proukakis, C. F. Barenghi, and C. S. Adams, Phys. Rev. Lett. **92**, 160403 (2004).
46. P. Nozieres and D. Pines: *The Theory of Quantum Liquids* (Perseus Publishing, New York, 1999).
47. E. Lundh, C.J. Pethick and H. Smith, Phys. Rev. A **55**, 2126 (1997).
48. D. S. Rokhsar, Phys. Rev. Lett. **79**, 2164 (1997).
49. E. Lundh, J. P. Martikainen, and K. A. Suominen, Phys. Rev. A **67**, 063604 (2003).
50. N. G. Parker and C. S. Adams, Phys. Rev. Lett. **95**, 145301 (2005); J. Phys. B **39**, 43 (2006).
51. S. Stringari, Phys. Rev. Lett. **77**, 2360 (1996).
52. A. Recati, F. Zambelli, and S. Stringari, Phys. Rev. Lett. **86**, 377 (2001).
53. S. Sinha and Y. Castin, Phys. Rev. Lett. **87**, 190402 (2001).
54. N.G. Parker, R.M.W. van Bijnen and A.M. Martin, Phys. Rev. A **73**, 061603(R) (2006).

55. K. W. Madison, F. Chevy, V. Bretin, and J. Dalibard, Phys. Rev. Lett. **86**, 4443 (2001).
56. J. E. Williams, E. Zaremba, B. Jackson, T. Nikuni, and A. Griffin, Phys. Rev. Lett. **88**, 070401 (2002).
57. F. Dalfovo and S. Stringari, Phys. Rev. A **63**, 011601(R) (2001).
58. T. Frisch, Y. Pomeau, and S. Rica, Phys. Rev. Lett. **69**, 1644 (1992).
59. T. Winiecki, J. F. McCann, and C. S. Adams, Phys. Rev. Lett. **82**, 5186 (1999).
60. B. Jackson, J. F. McCann, and C. S. Adams, Phys. Rev. Lett. **80**, 3903 (1998).
61. C. Raman, M. Köhl, R. Onofrio, D. S. Durfee, C. E. Kuklewicz, Z. Hadzibabic, and W. Ketterle, Phys. Rev. Lett. **83**, 2502 (1999).
62. R. Onofrio, C. Raman, J. M.Vogels, J. R. Abo-Shaeer, A. .P. Chikkatur, and W. Ketterle, Phys. Rev. Lett. **85**, 2228 (2000).
63. B. Jackson, J. F. McCann, and C. S. Adams, Phys. Rev. A **61**, 051603(R) (2000).
64. B. M. Caradoc-Davies, R. J. Ballagh, and K. Burnett, Phys. Rev. Lett. **83**, 895 (1999).
65. J. E. Williams and M. J. Holland, Nature **401**, 568 (1999).
66. A. E. Leanhardt, A. Görlitz, A. Chikkatur, D. Kielpinski, Y. Shin, D. E. Pritchard, and W. Ketterle, Phys. Rev. Lett. **89**, 190403 (2002).
67. N. S. Ginsberg, J. Brand, and L. V. Hau, Phys. Rev. Lett. **94**, 040403 (2005).
68. S. Komineas and N. Papanicolaou, Phys. Rev. A **68**, 043617 (2003).
69. R. G. Scott, A. M. Martin, T. M. Fromhold, and F. W. Sheard, Phys. Rev. Lett. **95**, 073201 (2005).
70. R. G. Scott, A. M. Martin, S. Bujkiewicz, T. M. Fromhold, N. Malossi, O. Morsch, M. Cristiani, and E. Arimondo, Phys. Rev. A **69**, 033605 (2004).
71. B. Jackson, J. F. McCann, and C. S. Adams, Phys. Rev. A **60**, 4882 (1999).
72. N. G. Berloff and C. F. Barenghi, Phys. Rev. Lett. **93**, 090401 (2004).
73. J. Ruostekoski and Z. Dutton, Phys. Rev. A **70**, 063626 (2005).
74. L. C. Crasovan, V. M. Pérez-García, I. Danaila, D. Mihalache, and L. Torner, Phys. Rev. A **70**, 033605 (2004).
75. T. P. Simula and P. B. Blakie, Phys. Rev. Lett. **96**, 020404 (2006).
76. Z. Hadzibabic, P. Krüger, M. Cheneau, B. Battelier, and J. Dalibard, Nature **441**, 1118 (2006).
77. M. J. Davis, S. A. Morgan, and K. Burnett, Phys. Rev. Lett. **66**, 053618 (2002).
78. N. G. Berloff and B. V. Svistunov, Phys. Rev. A **66**, 013603 (2002).
79. H. Lamb: *Hydrodynamics* (Cambridge University Press, 1932).
80. M. Tsubota, T. Araki, and S. K. Nemirovskii, Phys. Rev. B **62**, 11751 (2000).
81. K. W. Schwarz, Phys. Rev. B **31**, 5782 (1985).
82. J. Koplik and H. Levine, Phys. Rev. Lett. **71**, 1375 (1993).
83. M. Leadbeater, T. Winiecki, D. C. Samuels, C. F. Barenghi, and C. S. Adams, Phys. Rev. Lett. **86**, 1410 (2001).
84. M. Leadbeater, D. C. Samuels, C. F. Barenghi, and C. S. Adams, Phys. Rev. A **67**, 015601 (2003).
85. W. Thomson (Lord Kelvin), Philos. Mag. **10**, 155 (1880).
86. G. W. Rayfield and F. Reif, Phys. Rev. **136**, A1194 (1964).
87. A. A. Svidzinsky and A. L. Fetter, Phys. Rev. Lett. **84**, 5919 (2000).
88. B. Jackson, J. F. McCann, and C. S. Adams, Phys. Rev. A **61**, 013604 (2000).
89. E. Lundh and P. Ao, Phys. Rev. A **61**, 063612 (2000).
90. S. A. McGee and M.J. Holland, Phys. Rev. A **63**, 043608 (2001).

91. J. J. García-Ripoll and V. M. Pérez-García, Phys. Rev. A **63**, 041603 (2001).
92. J. J. García-Ripoll and V. M. Pérez-García, Phys. Rev. A **64**, 053611 (2001).
93. A. Aftalion and T. Riviere, Phys. Rev. A **64**, 043611 (2001).
94. P. Rosenbusch, V. Bretin, and J. Dalibard, Phys. Rev. Lett. **89**, 200403 (2002).
95. V. Bretin, P. Rosenbusch, F. Chevy, G. V. Shlyapnikov, and J. Dalibard, Phys. Rev. Lett. **90**, 100403 (2003).
96. A. L. Fetter, Phys. Rev. A **69**, 043617 (2004).
97. P. O. Fedichev and G. V. Shylapnikov, Phys. Rev. A **60**, R1779 (1999).
98. J. R. Abo-Shaeer, C. Raman, and W. Ketterle, Phys. Rev. Lett. **88**, 070409 (2002).
99. S. I. Davis, P. C. Hendry, and P. V. E. McClintock, Physica B **280**, 43 (2000).
100. D. P. Arovas and J. A. Freire, Phys. Rev. B **55**, 3104 (1997).
101. W. F. Vinen, Phys. Rev. B **61**, 1410 (2000).
102. E. Lundh and P. Ao, Phys. Rev. A **61**, 063612 (2000).
103. L. M. Pismen: *Vortices in Nonlinear Fields* (Clarendon Press, Oxford, 1999).
104. C. F. Barenghi, N. G. Parker, N. P. Proukakis, and C. S. Adams, J. Low. Temp. Phys. **138**, 629 (2005).
105. N. G. Berloff, Phys. Rev. A **69**, 053601 (2004).
106. B. M. Caradoc-Davies, R. J. Ballagh, and P. B. Blakie, Phys. Rev. A **62**, 011602 (2000).
107. A. Griesmaier, J. Werner, S. Hensler, J. Stuhler, and T. Pfau, Phys. Rev. Lett. **94**, 160401 (2005).
108. M. Marinescu and L. You, Phys. Rev. Lett. **81**, 4596 (1998).
109. S. Yi and L. You, Phys. Rev. A **61**, 041604 (2000).
110. K. Góral, K. Rzążewski, and T. Pfau, Phys. Rev. A **61**, 051601 (2000).
111. S. Yi and H. Pu, Phys. Rev. A **73**, 061602(R) (2006).
112. G. Oritz and D. M. Ceperley, Phys. Rev. Lett. **75**, 4642 (1995).
113. M. Sadd, G.V. Chester, and L. Reatto, Phys. Rev. Lett. **79**, 2490 (1997).
114. N. G. Berloff and P. H. Roberts, J. Phys. A **32**, 5611 (1999).
115. F. Dalfovo, Phys. Rev. B **46**, 5482 (1992).
116. J. Stuhler, A. Griesmaier, T. Koch, M. Fattori, T. Pfau, S. Giovanazzi, P. Pedri, and L. Santos, Phys. Rev. Lett. **95**, 150406 (2005).
117. D.H.J. O'Dell and C. Eberlein, Phys. Rev. A **75**, 013604 (2007).
118. D.H.J. O'Dell, S. Giovanazzi, and C. Eberlein, Phys. Rev. Lett. **92**, 250401 (2004).
119. C. Eberlein, S. Giovanazzi, and D.H.J. O'Dell, Phys. Rev. A **71**, 033618 (2005).
120. R.M.W. van Bijnen, D. H. J. O'Dell, N.G. Parker, and A.M. Martin, Phys. Rev. Lett. accepted, cond-mat/0602572 (2006).
121. C. Barceló, S. Liberati and M. Visser, Living Rev. Rel. **8**, 12 (2005).
122. W.G. Unruh, Phys. Rev. Lett. **46**, 1351 (1981).
123. W.G. Unruh, Phys. Rev. D **27**, 2827 (1995).
124. C. Barceló, S. Liberati and M. Visser, Class. Quant. Gav. **18**, 1137 (2001).
125. S.W. Hawking, Nature **248**, 30 (1974).
126. S.W. Hawking, Commun. Math. Phys. **43**, 199 (1975).
127. J.D. Bekenstein and M. Schiffer, Phys. Rev. **58**, 064014 (1998).
128. C. Barceló, S. Liberati, and M. Visser, Phys. Rev. A **68**, 053613 (2003).
129. T.R. Slatyer and C.M. Savage, Class. Quant. Grav. **22**, 3833 (2005).
130. S. Basak and P. Majumdar, Class. Quant. Grav. **20**, 2929 (2000).
131. S. Basak and P. Majumdar, Class. Quant. Grav. **20**, 3907 (2000).
132. F. Federici, C. Cherubini, S. Succi, and M.P. Tosi, Phys. Rev. A **73**, 033604 (2006).